Journal of Applied Fluid Mechanics, Vol. 16, No. 11, pp. 2101-2114, 2023.
Available online at www.jafmonline.net, ISSN 1735-3572, EISSN 1735-3645.
https://doi.org/10.47176/jafm.16.11.1897

Experimental Study on Wind Load and Wind-Induced Interference Effect of Three High-Rise Buildings

H. Cui[1,2,3], H. An[4], M. Ma[4], Z. Han[1,2,4], S. C. Saha[5] and Q. Liu[1,2,4,†]

[1] *State Key Laboratory of Mechanical Behavior and System Safety of Traffic Engineering Structures, Shijiazhuang Tiedao University, Shijiazhuang Hebei 050043, China*
[2] *Innovation Center for Wind Engineering and Wind Energy Technology of Hebei Province, Shijiazhuang Hebei 050043, China*
[3] *Department of Mathematics and Physics, Shijiazhuang Tiedao University, Shijiazhuang Hebei 050043, China*
4 School of Civil Engineering, Shijiazhuang Tiedao University, Shijiazhuang, Hebei 050043, China
[5] *School of Mechanical and Mechatronic Engineering, Faculty of Engineering and Information Technology, University of Technology Sydney, Ultimo NSW 2007, Australia*

†*Corresponding Author Email: qk@stdu.edu.cn*

ABSTRACT

Wind loads of high-rise buildings are a key parameter in architectural design. The magnitude and distribution characteristics of wind loads are of great importance for the safety and economy of structural design. The wind loads of high-rise buildings are quite different from those of monomer buildings. The wind-induced interference effect could significantly increase the local wind pressure of buildings, causing potential safety hazards for the main structure and enclosure structure. For the three common high-rise buildings, we adopted the wind tunnel test method to measure the surface pressure of each building. The corresponding *Re* number was 8.2×10^6. This paper studied the shape coefficients, fluctuating wind pressure coefficients and base bending moment coefficient of each building with different wind direction angles and different spacing ratios, and the maximum value of each parameter and the corresponding working condition were statistically analyzed. The results showed that, under any wind direction angle, the fluctuating wind pressure coefficients on all sides of the building were affected by the spacing ratio, and the fluctuation range was large. When the wind angle was 180º, the fluctuating wind pressure coefficients on the sides of Building 1 were most affected by the slope ratio. At this wind angle, the maximum value was 0.43 at a slope ratio of 5.0, which was 65% different from the minimum. Partition shape coefficients of some sides and top surfaces changed significantly with the spacing ratio. When the spacing ratio was 5.0, the base bending moment coefficients in the downwind and crosswind directions reached their maximum values, and the wind direction angles where the maximum values of the base bending moment coefficients in the downwind direction were 40º and 50º, respectively, and the wind direction angle where the maximum value of the base bending moment coefficients in the crosswind direction was 10º. Due to the influence of the wind angle and the building spacing ratio, the wind loads on the facades of the pyramidal group of buildings varied greatly, and the wind-induced interference effect was evident. The wind load between the building facades in the three buildings was different, and the wind disturbance effect was evident. Therefore, the most unfavorable stress state and interference state of the structure should be comprehensively considered in the wind resistance design of the three buildings. The building spacing ratio should preferably be set to 3.0, and wind angles of 10º, 40º, and 50º should be avoided whenever possible.

Article History

Received March 31, 2023
Revised July 18, 2023
Accepted July 19, 2023
Available online September 3, 2023

Keywords:

Base moment coefficient
Fluctuating wind pressure coefficients
Interference effect
Pyramidal group of buildings
Shape coefficients
Wind tunnel test

NOMENCLATURE

a	surface roughness coefficient	L	the distance between the three buildings
B	width of windward side of building	N	sampling number
C_p	wind pressure coefficient	Pi	time series of instantaneous pressure signal at measuring point
$C_{p,mean}$	average wind pressure coefficient	P_s	static pressure from reference point
$C_{p,rms}$	fluctuating wind pressure coefficient	U_s	wind speed at reference
C_M	average base bending moment coefficint	Z_i	the height of the measuring point from the ground
D	building cross section side length	α	wind angle
h	reference height	ρ	air density
H	model height	μ_{sdi}	the body shape coefficient
H_i	distance from the measuring point to the bottom of the model	μ_s	the partition body type coefficient of the partition plane

1. INTRODUCTION

Wind loads of tall buildings are a key design parameter, and their value and distribution characteristics are of great importance for the safety and economics of structural design. There are many high-rise buildings in modern cities. Due to the mutual interference of flow fields between buildings, the wind load on the surface of disturbed buildings is very different from that of individual buildings. The local wind pressure increases significantly on some facades, and may exceed that of the monomer (Huaying et al., 2015), causing safety issues in wind resistance design.

Yi et al. (2012) conducted an experimental study on the interference effect of high-rise buildings arranged in a staggered arrangement and found that the interference amplification effect of twisting towers in the middle position was very evident. Xiaobing et al. (2021) carried out wind tunnel tests on parallel three-square columns and studied the variation law of drag coefficient, wind pressure coefficient and Strouhal number of parallel three-square columns with spacing. An experimental study on the wind load characteristics of parallel three-square columns was conducted, and the results showed that columns arranged systemically on both sides could significantly interfere and increase the dynamic load of disturbed columns in the middle (Zhuangning et al., 2003). Bharat Singh et al. (2022) adopted high-rise buildings with rectangular sections as research objects and discussed the change of airflow pattern caused by the presence of disturbing buildings, thus leading to the change of wind pressure distribution. Kunyang et al. (2021) studied the average wind pressure around a single square column with different spacing ratios and showed that with changing wind angle, the average wind pressure distribution of each square column was similar to that of a single square column, and the average wind pressure coefficient in adjacent planes between square columns changed significantly (Kunyang, et al. 2021). Yaling et al. (2021) conducted a wind tunnel comparison test on super tall buildings, studied the static and dynamic interference effects of wind load on the main structure of the distributed high-rise buildings array and the interference effects of the envelope structure, and analyzed the interference mechanism combined with the Computational Fluid Dynamics calculation results and the basement bending moment spectrum. Rongqiang et al. (2022) numerically simulated the interference effect of cross-shaped super high-rise buildings, and the results showed that the surface shape coefficient of cross-shaped buildings was significantly affected by building spacing (Rongqiang et al., 2022). Liguo et al. (2021) performed a wind tunnel test on a high-rise building complex in the coastal area of Shenzhen and analyzed the mechanism of disturbance caused by the project building. Dongmei et al. (2012) used the World Financial Center in the Lujiazui area of Shanghai as a research object to conduct a wind tunnel test and studied the amplitude characteristics of the surface wind pressure coefficient and wind coefficient of each layer of super high-rise buildings under the interference from surrounding buildings. Lam et al. (2008) used wind tunnel test method to study the interference effect of a row of square high-rise buildings arranged nearby. The study showed that when the wind direction was about 30º, the wind flowed through the narrow building gap at high speed, thus generating a high negative pressure on the relevant building walls. Buildings in a row, therefore, did not exhibit a resonant response to wind at reduced velocities around 10 as an isolated square-plan tall building (Lam et al., 2008). Li & Li (2022) used CFD numerical simulation to study the influence of multi-high-rise buildings on the surface wind load characteristics of low-rise buildings. The research showed that wind pressure distribution on target low-rise buildings was very sensitive to changes in height ratio and space ratio. The average wind pressure coefficient and influence factor of low-rise buildings decreased with increasing height ratio and increase with increasing space ratio. The fluctuating pressure coefficient of the target low-rise building increased with the increasing height ratio, and the fluctuating pressure coefficient reaches the maximum when the height ratio was 8 (Li & Li 2022). Nagar et al. (2022) studied the interference effect of two buildings based on the mean interference factor and the root-mean-square interference factor, and the research showed that the maximum value of the mean interference factor was 4, 9 and 13, respectively, in the case of full blocking, half block and no block. In the case of complete blockage, the sidewall suction force was reduced by about 65 %. In all interference cases, the root-mean-square interference factor value was less than 1 (Nagar et al., 2022). Weifeng et al. (2022) studied the aerodynamic and structural

Table 1 Summary of previous studies on wind load on high-rise buildings

	High-rise building layout form	Main conclusion
Yi et al.	staggered	The torsion amplification of Tower 2 in the middle position was very significant, and the unfavorable wind direction was 110°.
Xiaobing et al.	juxtaposed	The aerodynamic forces of the square column on both sides were unequal, and the middle square column would be subjected to non-zero average lift force.
Yalin et al.	array	The average wind load in the translational direction of corner buildings was not higher than that of single buildings, but the average torque would increase greatly, and the transverse vibration may be strengthened.
Rongqian et al.	cross arrangement	The wind force on the windward and leeward sides of the occluded downstream buildings changed direction and decreased significantly.

dynamic characteristics of super-tall twin towers and compared them with isolated single towers. Research showed that when the twin towers were side by side in the wind, if the relative spacing was about 1.0 or less, the beneficial effect was pronounced, but when the relative spacing reached 2.0, it could be ignored. When towers were configured in conjunction with the wind, the beneficial effect would remain in effect until the maximum relative spacing tested was 2.0 (Weifeng et al., 2022).

Rongyang et al. (2022) used the Boltzmann method (IB-LBM) to study the influence of Reynolds number (*Re*) and clearance rate on the flow characteristics, force coefficient and Strouhal number (St) of three rounded square columns arranged in a square-shape pattern in low Re number (Rongyang et al. 2022). Chun yan et al. (2011) numerically simulated the static interference effect of shaped buildings under a specific inflow direction and studied the distribution law of wind pressure interference factors on the surface of the disturbed buildings.

From the research point of view, studies on buildings with a square-shaped plan were few, and the influencing factors were relatively simple. Only the wind load distribution characteristics of a building under a specific wind angle were studied. However, the wind load and wind disturbance effect of different building facades in different inflow direction was not the same as these three common high-rise buildings.

As shown in Table 1, the wind load and the interference effect of high-rise buildings were mainly studied in staggered, juxtaposed, inclined, conjoined and crossed arrangements. Therefore, the influence of various flow directions, different building spacing ratios, the surface shape coefficient, fluctuating wind pressure coefficient and the basement bending moment coefficient of all buildings were all studied by the wind tunnel test in this paper, in order to provide some reference for the wind-resistant design of high-rise buildings.

2. OVERVIEW OF WIND TUNNEL TEST

2.1 Test Model and Measurement Point Arrangement

The research object is a pyramidal group of 33-story residential buildings commonly seen in China. The three buildings are all 20 m in cross-section length and 100 m in height. The test model is a rigid pressure measurement model made of Acrylonitrile-butdiene-styrene plate with a scale ratio of 1:200. In the actual building, the Re number at 10m high is 8.2×10^6. Figure 1 shows the building layout and wall numbering. For example, the numbering of each facade and upper surface of Building 1 is I, F, G, H and J, respectively. The spacing ratio of the three buildings *L/D* (L is the central link of the three buildings, D is the lateral length of the cross section of the buildings) is 2.5, 3.0, 3.5, 4.0 and 5.0. The wind angle α ranges from 0° to 180°, with an interval of 10°. There are 19 wind angles, which are achieved by rotating the model clockwise.

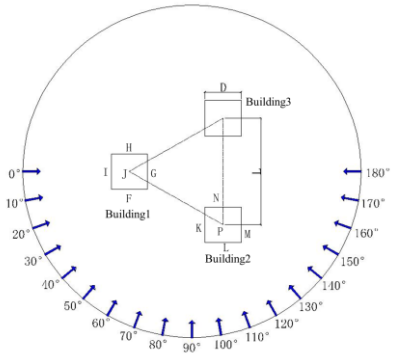

Fig. 1 Model placement and wind direction angles

The layout and pressure hole size of the model are shown in Fig. 2. The pressure holes are arranged around and on the top surface of Building 1 and Building 2. Sixteen pressure holes are selected at the top of the building model and forty-five pressure holes are arranged on each building facade.

2.2 Test Site

The experiment is carried out in the low-speed experimental area of the Wind Tunnel Laboratory of Shijiazhuang Tiedao University The center of the turntable in this test section is 4.4 m wide, 3.0 m high and 24.0 m long, and the wind speed ranges from 1.0 m/s to 30.0 m/s (Qingkuan, 2011). Rough element and wedge are used to simulate the atmospheric boundary layer wind field in the test. The test results are consistent with Class C landforms in code GB50009-2012 for loading on building structures (GB50009 Load code for the design of building structures, 2012). Figure 3 shows the test model and the wind tunnel test environment, among which the three blue square columns are the pin-shaped tall building

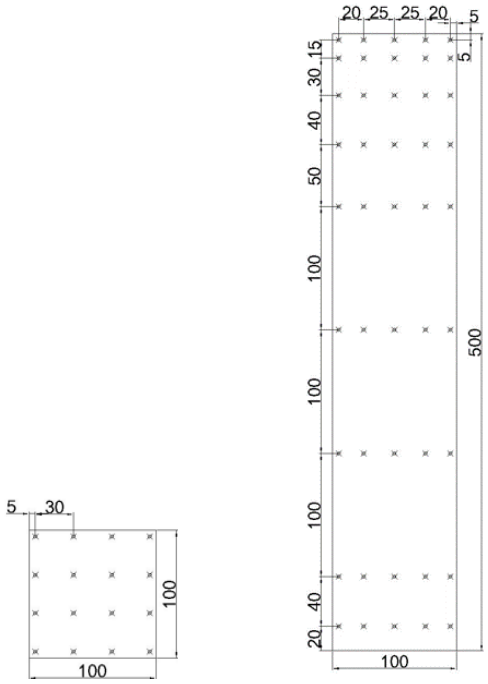

(a) Top surface (b) Elevation

Fig. 2 Arrangement and dimension drawing of pressure holes on the surface of building model(mm)

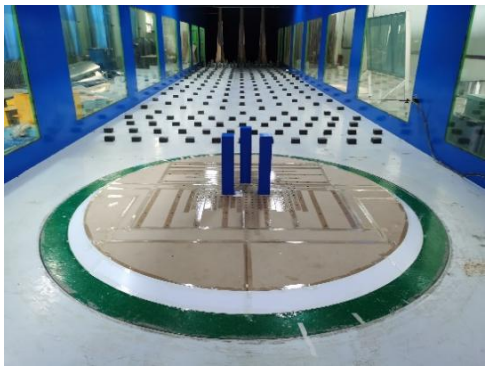

Fig. 3 Experimental model and environment

complex model. The wind speed of the inflow in the wind tunnel laboratory and the wind pressure of the measurement points on the model surface are measured by the Cobra anemometer and the electronic pressure sweep valve, respectively.

3. PARAMETER DEFINITION AND DATA VALIDATION

3.1 Parameter Definition

The wind pressure distribution of the building surface under different working conditions is represented by the dimensionless wind pressure coefficient C_p, which is defined as follows:

$$C_p(i) = \frac{P_i - P_s}{\frac{1}{2}\rho U_s^2} \tag{1}$$

Where, P_i is the time series of the instantaneous pressure signal measured at a measurement point on the surface of the model, P_s is the static pressure value at the reference point, ρ is the air density, U_s is the wind speed at the reference point.

The average wind pressure coefficient $C_{p,mean}$, and the fluctuating wind pressure coefficient $C_{p,rms}$ at the measurement point are defined as Eq. (2) and Eq. (3), respectively:

$$C_{p,mean} = \frac{\sum_{i=1}^{N} C_p(i)}{N} \tag{2}$$

$$C_{p,rms} = \sqrt{\frac{\sum_{i=1}^{N} (C_p(i) - C_{p,mean})^2}{N-1}} \tag{3}$$

Where, N is the number of sampling points. The number of sample points in this experiment is 9,900.

The body shape coefficient μ_{sdi} at the measurement point can be calculated from the average wind pressure coefficient by Eq. (4):

$$\mu_{sdi} = \frac{C_{p,mean}}{(Z_i / h)^{2\alpha}} \tag{4}$$

Where, μ_{sdi} is the body shape coefficient at measurement point i; Z_i is the height at the measurement point i; h is the height of the reference point; Is the ground roughness index, according to the current codes for building structure load, the C-type geomorphology α is 0.22.

The area around each surface measurement point was partitioned and the area weighted average of the body shape coefficient of the measurement point was performed to obtain the body shape coefficient of the surface zone μ_s, as shown in Eq. (5):

$$\mu_s = \frac{\sum \mu_{sdi} A_i}{\sum A_i} \tag{5}$$

Where, μ_s is the partition body type coefficient of the partition plane, A_i is the sub-partition area, and μ_{sdi} is the partition body type coefficient of the sub-partition.

For the analysis of the whole building, the dimensionless average bending moment coefficient CM of the base along and transversely to the wind direction is defined, as shown in Eq (6):

$$(6): C_M = \frac{\sum_i p_i A_i H_i}{\frac{1}{2}\rho U_r^2 H^2 B} \tag{6}$$

Where, C_M is the average base bending moment coefficient, H_i is the distance from the measurement point to the bottom of the model, H is the model height, and B is the area of vertical projection between the building and the incoming flow.

3.2 Date Validation

Numerical simulation was performed when the spacing ratio was 2.5 and the wind direction was 0 degree, the wind pressure coefficient at the same height was

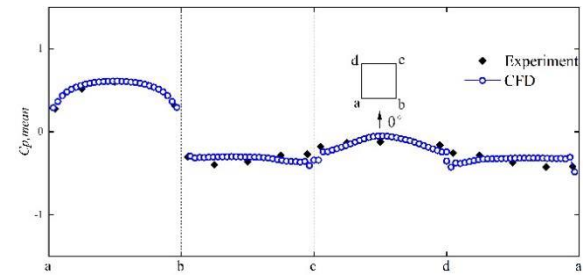

(a) Building 1

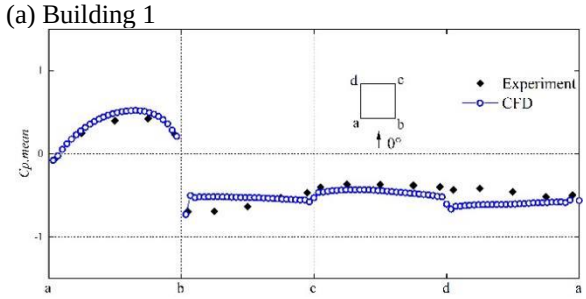

(b) Building 1

Fig. 4 Comparison between experiment data and numerical simulation of wind pressure coefficient

selected for comparison. As shown in Fig. 4, the distribution law and size of the wind pressure coefficient are basically the same. There is some difference between the crosswind side and the leeward side of Building 2, which can be caused by the relatively unstable flow field behind Building 2. However, the difference is within the acceptable range, which proves that the results of this test are accurate and reliable.

4. ANALYSIS OF THE PARTITION SHAPE COEFFICIENT

4.1 Partition Shape Coefficient of Building 1

Figure 5 shows the zoned body type coefficient of Plane I of Building 1 under different spacing ratios and wind angles. The Plane I zoned body type coefficient shows the same variation rule under different spacing ratios. The zoned body type coefficient decreases in the range of $0° \le \alpha \le 80°$ and $160° \le \alpha \le 180°$, and increases in the range of $80° \le \alpha \le 160°$. When the wind direction is $0° \le \alpha \le 50°$, the zoned shape coefficient is positive; when the wind direction is $60° \le \alpha \le 180°$, the zoned shape coefficient is negative. The zonal body type coefficient of this plane is very little affected by the spacing ratio. When $\alpha \ge 90°$, the zonal body type coefficient of this plane begins to change obviously with the spacing ratio, but the range of change is still small.

Figure 6 shows the contour map of the body shape coefficient when the spacing ratio L/D = 2.5. When the wind direction is 30°, negative pressure begins to appear in the left area of Plane I. The increase in the wind direction angle causes Plane I to gradually transform from the windward state to the lateral state. The formation of the shear layer in Plane I leads to a negative pressure on this surface.

Figure 7 shows the zoned body type coefficient of Plane F of Building 1 under different spacing ratios and wind angles. The zoned body type coefficient of Plane F

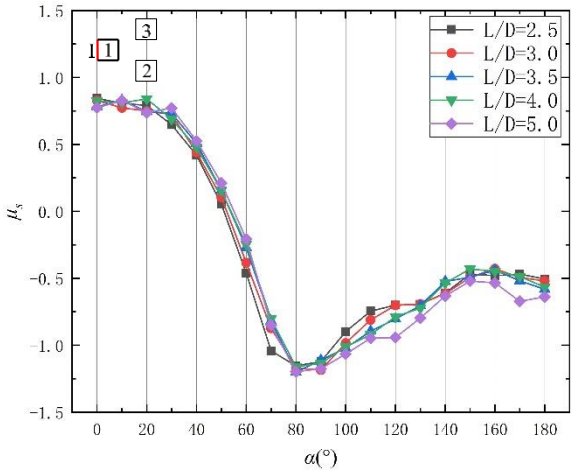

Fig. 5 Variation of Plane I partition shape coefficient of Building 1 with different spacing ratios and wind direction angles

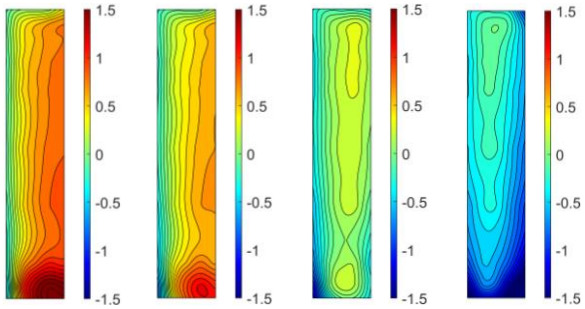

(a) α=30° (b) α=40° (c) α=50° (d) α=60°

Fig. 6 Isogram of shape coefficient of Plane I of Building 1 with spacing ratio of 2.5

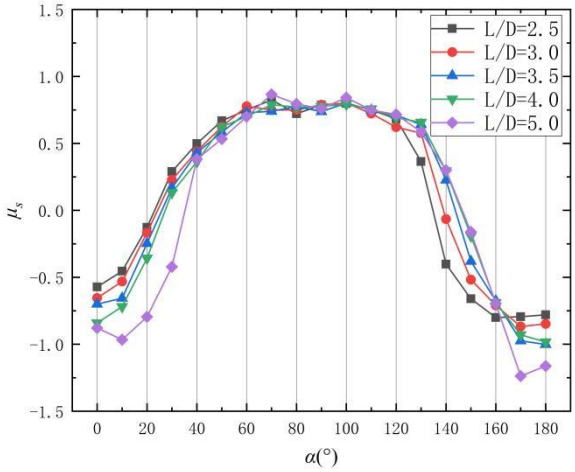

Fig. 7 Variation of Plane I partition shape coefficient of Building 1 with different spacing ratios and wind direction angles

shows the same variation rule of wind direction angle under different spacing ratios. In the range of the wind direction angle $0° \le \alpha \le 70°$, the zoned body type coefficient shows an increasing trend; in the interval of $70° \le \alpha \le 100°$, the zoned body type coefficient basically remains unchanged at about 0.75. In the scale of $100° \le \alpha \le 180°$, the zonal body type coefficient showed a decreasing trend. The zoned shape coefficient shows a

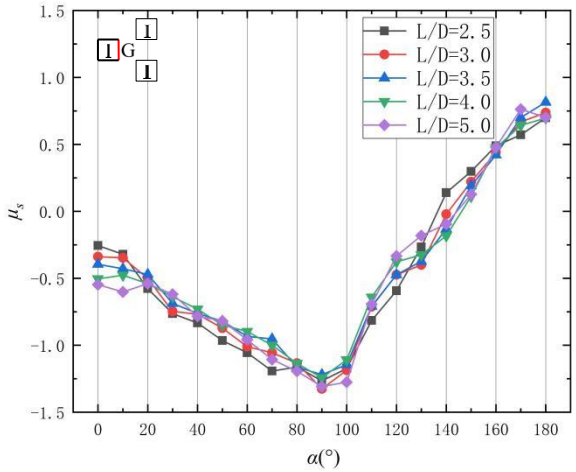

Fig. 8 Variation of Plane G partition shape coefficient of Building 1 with different spacing ratios and wind direction angles

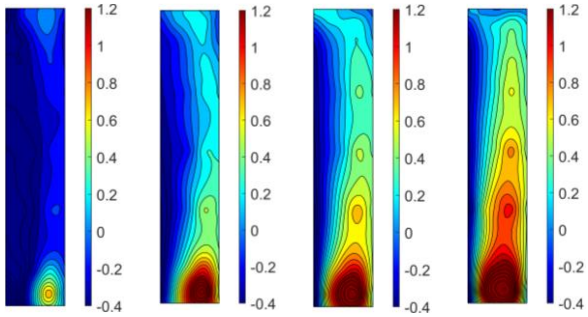

(a) α=130° *(b)* α=140° *(c)* α=150° *(d)* α=160°

Fig. 9 Isogram of shape coefficient of Plane G of Building 1 with spacing ratio of 2.5

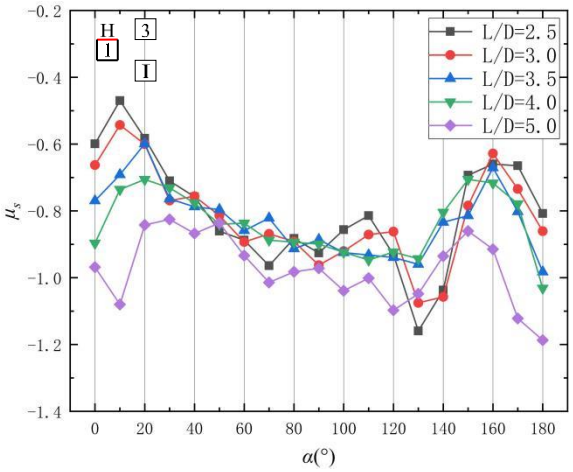

Fig. 10 Variation of Plane H partition shape coefficient of Building 1 with different spacing ratios and wind direction angles

decreasing trend. Within the range of $0° \le \alpha \le 60°$, the zoned shape coefficient decreases with an increasing spacing ratio under the same wind direction. Within the limit of $0° \le \alpha \le 20°$, because the zoned shape coefficient is negative, the whole building facade is subject to negative pressure and the interference of the building group in Plane F is favorable. Within the range of $30° \le \alpha \le 60°$, the interference of building group on Plane F is adverse interference. When the wind angle is $130° \le \alpha \le 160°$, the zoned shape coefficient increases with an increasing spacing ratio at the same wind angle. In the interval of $170° \le \alpha \le 180°$, it decreases with increasing spacing ratio, and the variation law of body shape coefficient with spacing ratio changes after 160°. This is because in the range of $160° \le \alpha \le 180°$, the smaller the spacing ratio, the more obvious the shielding effect of Building 2 on Building 1.

Figure 8 shows the zoned body type coefficient of Plane G of Building 1 under different spacing ratios and wind angles. The zoned body type coefficient of Plane G has the same variation rule under different spacing ratios. The zoned body type coefficient decreases in the scale of $0° \le \alpha \le 90°$ and increases in the range of $90° \le \alpha \le 180°$. When the wind direction is $0° \le \alpha \le 140°$, the zoned body type coefficient is negative; when the wind direction is $140° \le \alpha \le 180°$, the zoned body type coefficient is positive. The change in wind angle caused the Plane G to gradually shift from leeward to windward side. When the wind direction is 90°, the maximum negative pressure is -1.33. The drag force due to the large negative pressure will not only cause the structure to be affected by torque and the large torque on the structure, but also can cause the tiles to fall off. Therefore, the building should avoid the occurrence of this wind direction.

Figure 9 shows the body shape coefficient contour map when the spacing ratio *L/D* = 2.5. When the wind direction is 130°, positive pressure starts to appear in the right area of Plane G. As the angle increases, the positive pressure area begins to develop to the left. This is due to the obstructive effect of Building 2, which generates vortices in Plane G, making it present a state of negative pressure. As the wind direction angle increases, this obstructive effect decreases and the incoming wind acts directly on the facade, starting to appear areas of positive pressure.

Figure 10 shows the zoned body type coefficient of Plane H of Building 1 under different spacing ratios and wind angles. The zoned shape coefficient of Plane H is negative under different spacing ratios and wind angles. Due to the interference effect of Buildings 2 and 3 on Building 1 and the existence of vortex shedding, the flow field around this facade is complicated, and the zoned shape coefficient of this facade does not show regularity as a whole. When the spacing ratio is 2.5 and 3.0, and the wind direction is 130°, the zonal shape coefficient drops, due to the slit effect of Building 3 on Plane H, resulting in large negative pressure at this time. When the wind angle is 0°, 10° and 180°, the zoned shape coefficient decreases with increasing spacing ratio. The interference effect between the buildings is favorable for Plane H. The zoned shape coefficient at 180° is less than at 0° at the same spacing ratio, because Plane H is in the downstream area at 180° and there is a more evident slit effect at this time.

Figure 11 shows Plane J of Building 1 under different spacing ratios and wind angles plane partition type coefficient. The average body shape coefficients of Plane

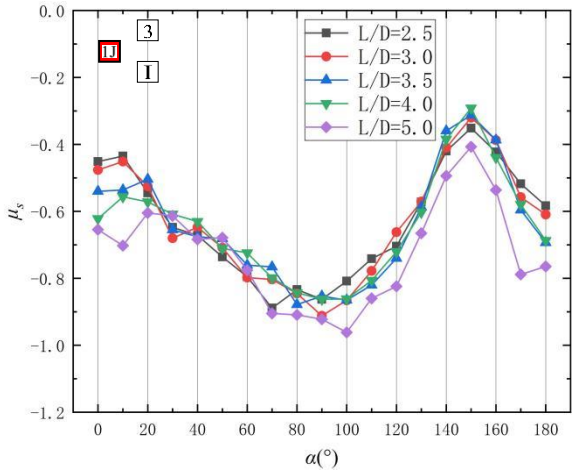

Fig. 11 Variation of Plane J partition shape coefficient of Building 1 with different spacing ratios and wind direction angles

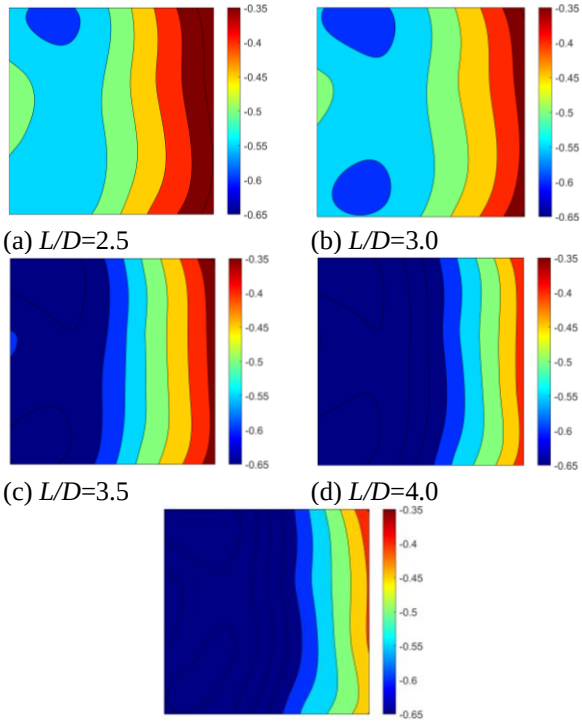

Fig. 12 Isogram of Plane J shape coefficient of Building 1 under wind direction angle of 0 °

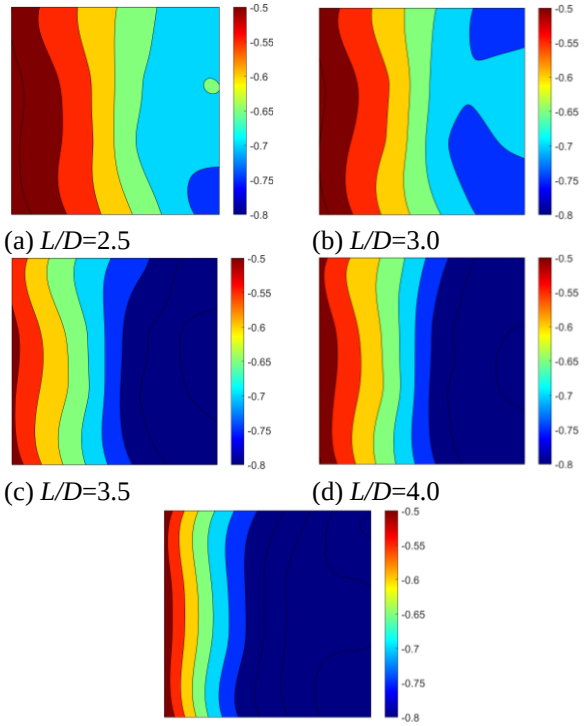

Fig. 13 Isogram of Plane J shape coefficient of Building 1 under wind direction angle of 180 °

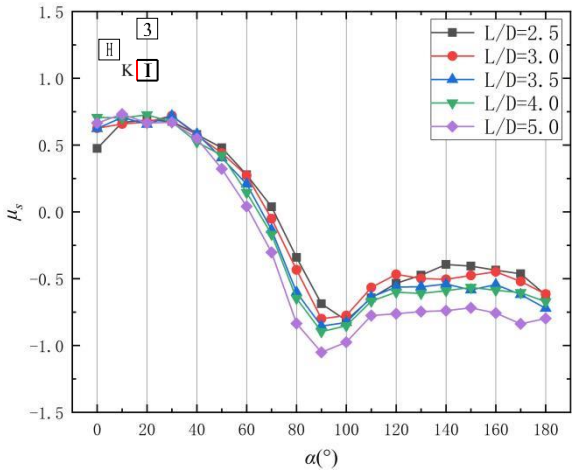

Fig. 14 Variation of Plane K partition shape coefficient of Building 2 with different spacing ratios and wind direction angles

J at different spacing ratios and wind angles are negative. Except for the four wind angles of 0°, 10°, 170° and 180°, the zoned body type coefficients did not change much with the distance ratio under the same wind direction, and the overall change trend of the zoned body type coefficients under different distance ratios are first decreased, then increased, and then decreased. Under the four wind angles of 0°, 10°, 170° and 180°, the zoned shape coefficient decreases with increasing spacing ratio, that is, negative pressure increases.

Figure 12 is the contour map of Plane J body type coefficient of Building 1 with wind angle 0°, and Figure 13 is the contour map of Plane J body type coefficient of Building 1 with wind angle of 180°. Under wind angle 0° and 180°, the body type coefficient gradually decreases, that is, negative pressure increases, and the area of a larger negative pressure gradually increases, resulting in a decrease in the average body type coefficient (Fig. 12 and Fig. 13).

4.2 Partition Shape Coefficient of Building 2

Figure 14 shows the zoned body type coefficient of Plane K of Building 2 under different spacing ratios and wind angles. A comparative analysis of Fig. 14 and Fig. 5, that is, a comparison between Plane K of Building 2 and Plane I of Building 1, shows that the zoned body type coefficient basically has the same tendency to

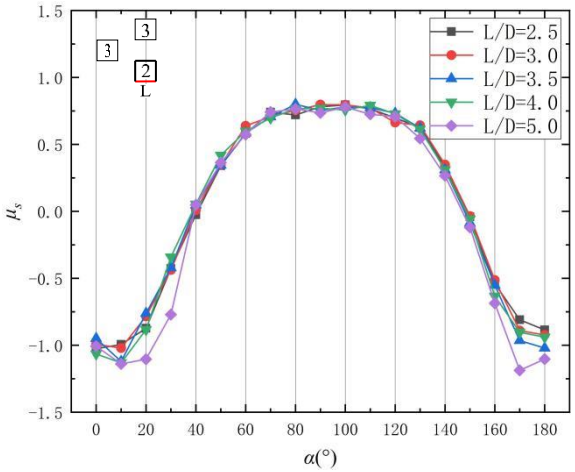

Fig. 15 Variation of Plane L partition shape coefficient of Building 2 with different spacing ratios and wind direction angles

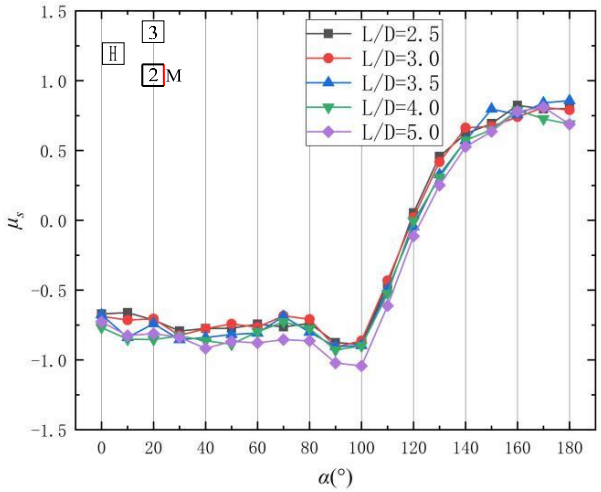

Fig. 16 Variation of Plane M partition shape coefficient of Building 2 with different spacing ratios and wind direction angles

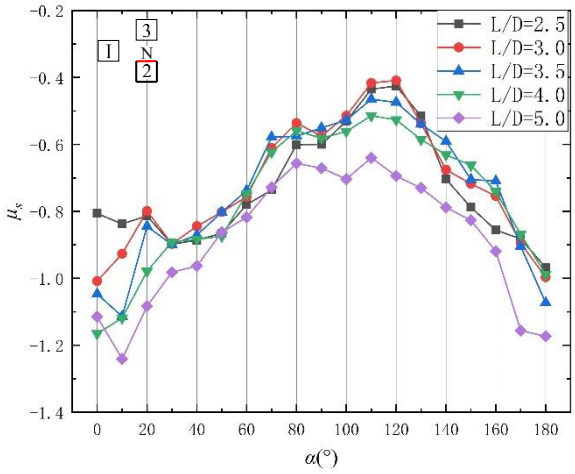

Fig. 17 Variation of Plane N partition shape coefficient of Building 2 with different spacing ratios and wind direction angles

change the wind direction angle, showing a trend of first decreasing and then increasing. The difference is that when the wind angle is greater than 90°, the Plane K zonation coefficient decreases with the increase in the spacing ratio at the same wind angle, that is, the negative pressure increases, indicating that the interference effect from Plane K of Building 1 to Building 2 begins to appear when the wind angle is greater than 90°, and this interference is a favorable interference. Plane K is more affected by the spacing ratio than Plane I. This is because the Plane K is constantly in a disturbed state. That is, at low angles, the inflow will be affected by the shear layer and wake flow from Building 1; At high angles, the wake flow measured in Plane K will be obstructed by Building 1, hence the different values.

Figure 15 shows the zonal body type coefficient of Plane L of Building 2 under different spacing ratios and wind angles. A comparative analysis between Fig. 15 and Fig. 7, that is, a comparison between Plane L of Building 2 and Plane F of Building 1, shows that the wind direction angle of the zoned shape coefficient is basically the same, with a general trend of first increasing and then decreasing. For *L/D*=5, the wind direction at low and high angles, there is a shear layer in Plane L and Plane K. Due to the slight change in the wind direction angle, the strength of the shear layer increases and becomes closer to the wall, resulting in an increase in negative surface pressure, that is, the zoned shape coefficient appears with the lowest value. As the wind develops in the direction perpendicular to the wall, the wall begins to show positive pressure, which increases the zoned shape coefficient.

Figure 16 shows the zoned shape coefficient of Plane M of Building 2 under different spacing ratios and wind angles. Comparing Fig. 16 with Fig. 8, that is, comparing Plane M of Building 2 with Plane G of Building 1, the zoned shape coefficient of Plane M of Building 2 basically changes with the angle inside from the range of $0° \le \alpha \le 80°$, remaining at about 0.75. This is because Plane M is less disturbed than Plane G. In the interval of $0° \le \alpha \le 40°$, the zoned shape coefficient of Plane G is less than 0.75, which is a favorable interference.

In the range of $40° \le \alpha \le 80°$, the zoned shape coefficient of Plane G is greater than 0.75, which is adverse interference.

Figure 17 shows the zoned body type coefficients of Plane N of Building 2 under different spacing ratios and wind angles. The zoned body shape coefficients of Plane N at different spacing ratios and wind direction angles are all negative, that is, Plane N is subjected to wind suction in the range of $0° \le \alpha \le 180°$, and the general trend is first increasing and then decreasing. This plane is subject to both the occlusion effect and the slit effect, which makes the variation law of the zoned body type coefficient of this plane with the spacing ratio not significant. However, when the spacing ratio is 5.0, the zoned body type coefficient is smaller in most cases, and when the wind direction is 0°, the zoned body type coefficient is greater when the spacing ratio is 5.0 than when the spacing ratio is 4.0.

Figure 18 shows the zoned shape coefficient of Plane P of Building 2 under different spacing ratios and wind angles. The zoned shape coefficient of Plane P under

Table 2 Maximum value of the average shape coefficient of each face of Building 1

Elevation	Spacing ratio(*L*/*D*)	Wind angle (°)	Maximum value	Spacing ratio (*L*/*D*)	Wind angle (°)	Minimum value
F	5.0	70	0.866	5.0	170	-1.237
G	3.5	180	0.815	3.0	90	-1.326
H	2.5	10	-0.470	5.0	180	-1.187
I	2.5	0	0.845	3.5	80	-1.202
J	4.0	150	-0.292	5.0	100	-0.962

Table 3 Maximum value of the average shape coefficient of each face of Building 2

Elevation	Spacing ratio (*L*/*D*)	Wind angle (°)	Maximum value	Spacing ratio (*L*/*D*)	Wind angle (°)	Minimum value
L	3.5	80	0.800	5.0	170	1.188
M	3.5	180	0.857	5.0	100	-1.043
N	3.0	120	-0.409	5.0	10	-1.241
K	5.0	10	0.732	5.0	90	1.051
P	3.0	120	-0.431	5.0	170	0.860

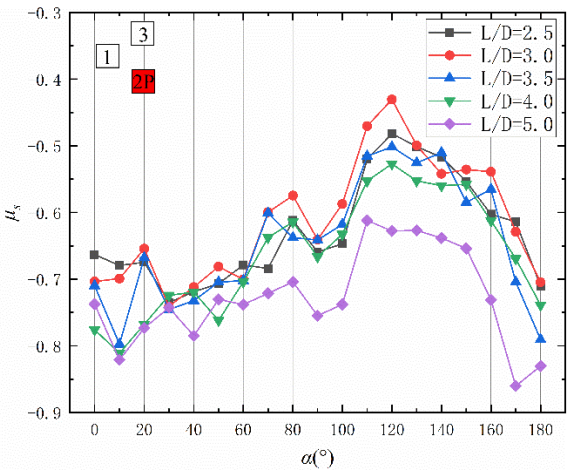

Fig. 18 Variation of Plane P partition shape coefficient of Building 2 with different spacing ratios and wind direction angles

different spacing ratios and wind angles is negative, that is, all Planes P are subject to wind suction within the range of $0° \leq \alpha \leq 180°$, and the variation of zoned shape coefficient of Plane P presents nonlinear.

Designers usually pay attention to structure stress under the most unfavorable conditions. Based on the above broken-line diagram of the zoned body type coefficient of each building under different working conditions, the maximum positive pressure and maximum negative pressure of Building 1 and Building 2 can be obtained under which working conditions are shown in Table 2 and Table 3. When the facade is perpendicular to the inflow direction due to interference between buildings, the average body shape coefficient does not show the maximum or minimum state (Table 2 and Table 3). Therefore, systematic wind load research should be carried out when designing the wind load of this special arrangement of high-rise buildings.

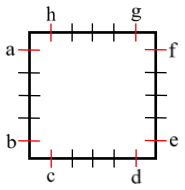

Fig. 19 Number diagram of measuring points

5. ANALYSIS OF FLUCTUATION WIND PRESSURE COEFFICIENT

To study the influence of wind load on the building envelope, the fluctuating wind pressure coefficient of the building is analyzed. Measurement points above 360 mm from the ground (That is, 2/3H from the ground, where H is the model height) are selected for the survey (Zheng et al., 2011). To represent the fluctuating wind pressure coefficient of the measurement points on each surface are numbered as shown in Fig. 19. Figure 20 to Fig. 25 show the fluctuating wind pressure coefficients of each building at different spacing ratios and wind angles. Fluctuating wind pressure coefficients at wind angles of 0°, 90° and 180° are selected for analysis.

5.1 Fluctuating Wind Pressure Coefficient of Building 1

As shown in Fig. 20, at a wind angle of 0°, the fluctuating wind pressure coefficient of each facade of Building 1 is the minimum when the spacing ratio is 3.0 and the maximum when the spacing ratio is 4.0. However, changing the spacing ratio does not affect the distribution law of the fluctuating wind pressure coefficient of each facade. The maximum values of the fluctuating wind pressure coefficient on the leeward side I and on the leeward side G both occur at the midpoint of the measurement, indicating that the vortices formed on the leeward side are relatively stable. The maximum fluctuating wind pressure coefficient for both sides appears at the lateral measurement point, due to a slight

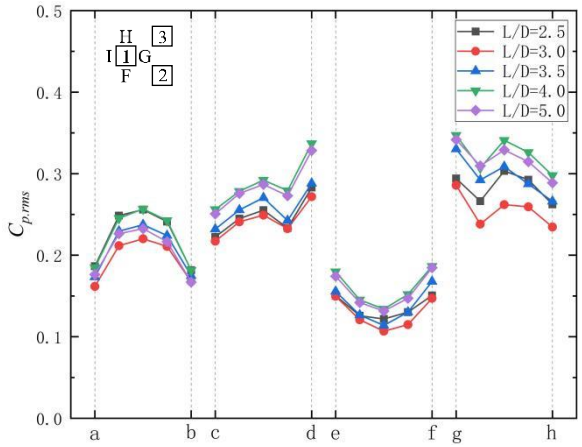

Fig. 20 Fluctuating wind pressure coefficient of Building 1 at 0 degree wind direction angle on each elevation

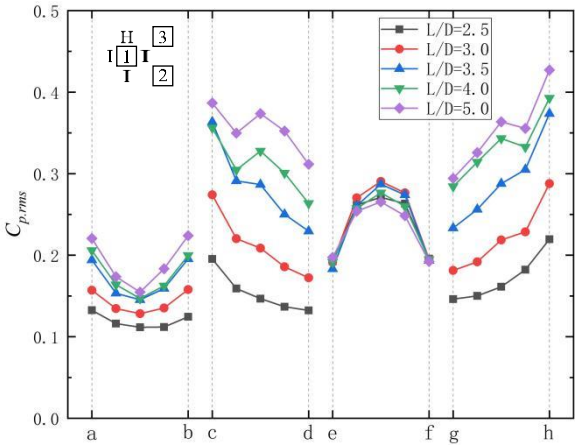

Fig. 22 Fluctuating wind pressure coefficient of Building 1 at 180 degree wind direction angle on each elevation

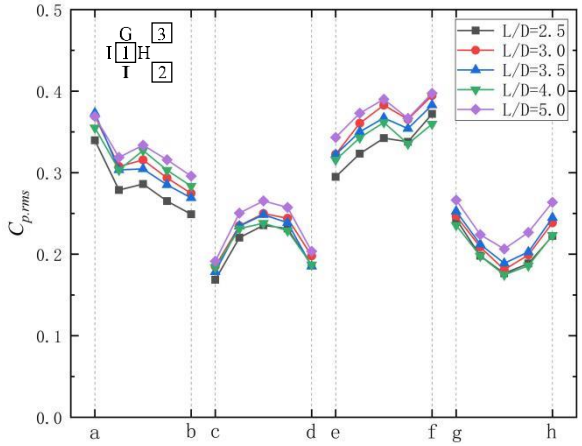

Fig. 21 Fluctuating wind pressure coefficient of Building 1 at 90 degree wind direction angle on each elevation

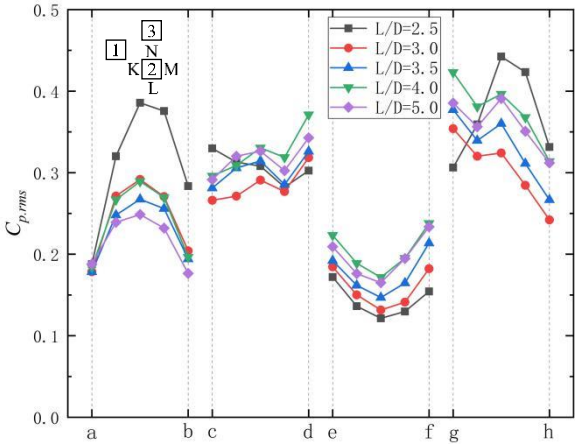

Fig. 23 Fluctuating wind pressure coefficient of Building 2 at 0 degree wind direction angle on each elevation

wake oscillation at the rear corner of the side of Building 1. Compared to the other three elevations, Plane H is more affected by the spacing ratio, and the maximum fluctuating wind pressure coefficient difference is 0.079.

Figure 21 shows that under a wind direction angle of 90°, the maximum fluctuating wind pressure coefficient of each facade of Building 1 occurs when the spacing ratio is 5.0. As Plane F is the windward side and Plane H is the leeward side, the maximum value of the fluctuating wind pressure coefficient is at the middle measurement point, and the maximum value of the two sides I and H appear at the side measurement point. The four elevations of the fluctuating wind pressure coefficient are less affected by the spacing ratio. Comparing with Fig. 19, the windward, and leeward sides have the same variation rules. That is, Plane F is the windward side, Planes I and G are the crosswind side, and Plane H is the leeward side.

As shown in Fig. 22, under the wind angle of 180°, Building 1 is in the downstream area of the inflow and is greatly affected by the occlusion effect and slit effect of Building 2 and Building 3. Except for Plane G, the ripple wind pressure coefficients of the other three facades are greatly affected by the spacing ratio, and the ripple wind pressure coefficients of Plane I, F and H gradually decrease with decreasing spacing ratio. Interference from building groups to Building 1 is a favorable one. This is because Building 1 is located in the downstream region of the group, which is heavily affected by slit effects, screening effects, and the wake from the upstream buildings. Increasing the building spacing ratio slightly increases the rift effect and decreases the blocking effect. As a result, the lateral fluctuating wind pressure coefficient increases significantly as the spacing ratio increases. However, when the spacing ratio increases to a certain extent, the flow pattern becomes more and more similar to that of a monomer and the slit effect weakens, so that the fluctuating wind pressure coefficient decreases as the spacing ratio increases.

5.2 Fluctuating Wind Pressure Coefficient of Building 2

A comparative analysis of Fig. 23 and Fig. 20 shows that when the wind direction is 0°, the fluctuating wind pressure coefficient of Building 2 at the interval ratio of 2.5 changes greatly. The fluctuating wind pressure coefficient of Plane K at the interval ratio of 2.5 is significantly higher than at other interval ratios, with the maximum value reaching 0.386. Compared to other spacing ratios, the variation law of fluctuating wind

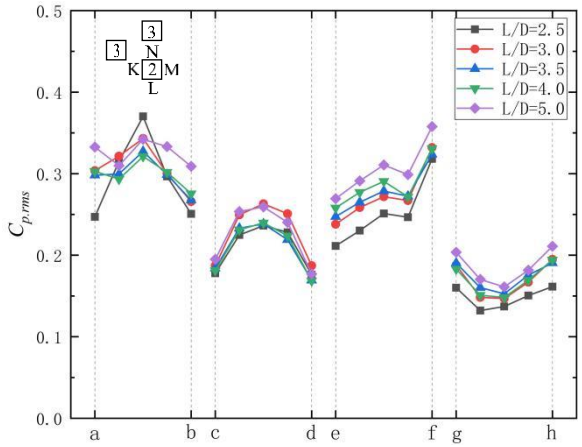

Fig. 24 Fluctuating wind pressure coefficient of Building 2 at 90 degree wind direction angle on each elevation

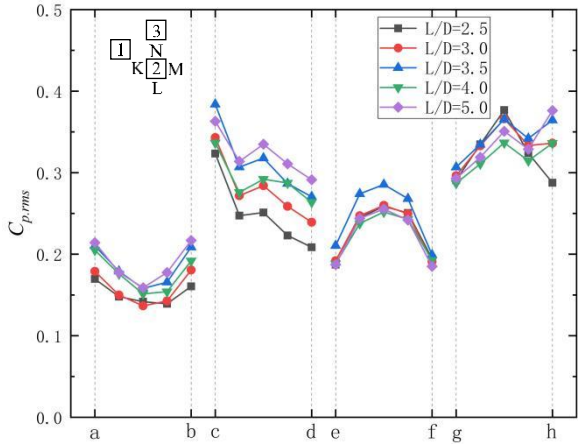

Fig. 25 Fluctuating wind pressure coefficient of Building 2 at 180 degree wind direction angle on each elevation

pressure coefficient of Planes L and H with the spacing ratio of 2.5 changes greatly with the position of the measurement point. This is because Building 2 is in the downstream area when the wind direction is 0° and the interference is severe when the spacing ratio is 2.5. Vortices will be generated in the lateral region, causing large changes in the flow field.

A comparative analysis of Fig. 24 and Fig. 21 shows that when the wind direction is 90°, the fluctuating wind pressure coefficient of Plane K measurement point of Building 2 does not show regularity, and the maximum fluctuating wind pressure coefficient under different spacing ratios appear all at the middle of measurement point, while the variation law of the fluctuating wind pressure coefficient of the other three facades, together with the spacing ratio, is consistent with that of Building 1.

A comparative analysis of Fig. 25 and Fig. 22 shows that when the wind direction is 180°, the fluctuating wind pressure coefficient of Building 2 on each face is less affected by the spacing ratio than that of Building 1. This is because when the wind direction is 180°, Building 2 is at the top of the inflow and is less affected by interference between buildings. There is a slit effect between Plane N

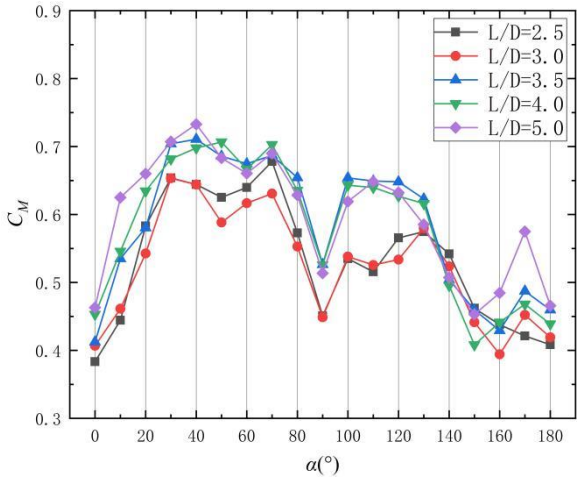

Fig. 26 Bending moment coefficient of downwind foundation of Building 1 at different spacing ratios and different wind directions

of Building 2 and Building 3, so the variation rule of fluctuating wind pressure coefficient of Plane N is different from that of Plane H of Building 1.

6. ANALYSIS OF THE BENDING MOMENT COEFFICIENT OF BASE

6.1 Average Downwind Bending Moment Coefficient to the Base

Figure 26 shows the bending moment coefficient of Building 1 downwind to the base under different spacing ratios and wind angles. In the wind direction range of Building 1: $0° \le \alpha \le 30°$, $70° \le \alpha \le 100°$, $130° \le \alpha \le 150°$, the variation law of bending moment coefficient downwind base under different spacing ratios is basically the same. In the wind direction ranges of $30° \le \alpha \le 70°$ and $100° \le \alpha \le 130°$, the bending moment coefficients of downwind base with spacing ratios of 2.5 and 3.0 are significantly different from those with spacing ratios of 3.5, 4.0 and 5.0, and the maximum difference is 0.132. The maximum downwind bending moment coefficient toward the base of Building 1 is 0.733, the spacing ratio is 5.0, and the wind direction angle is 40°.

Figure 27 shows the bending moment coefficient of Building 2 in the wind direction to the base under different spacing ratios and wind angles. The variation trend of the downwind base bending moment coefficient is basically the same as the angle of Building 2 at different spacing ratios. Compared to Building 1, there is no significant difference between the downwind base bending moment coefficients at different spacing ratios in the range of $30° \le \alpha \le 70°$ and $100° \le \alpha \le 130°$. The maximum downwind base bending moment coefficient of Building 2 is 0.695, the spacing ratio is 5.0, and the wind direction angle is 50°.

6.2 Average Transverse Bending Moment Coefficient to the Base

Figure 28 shows the transverse bending moment coefficient of the wind base of Building 1 under different spacing ratios and wind angles. In Building 1, within the

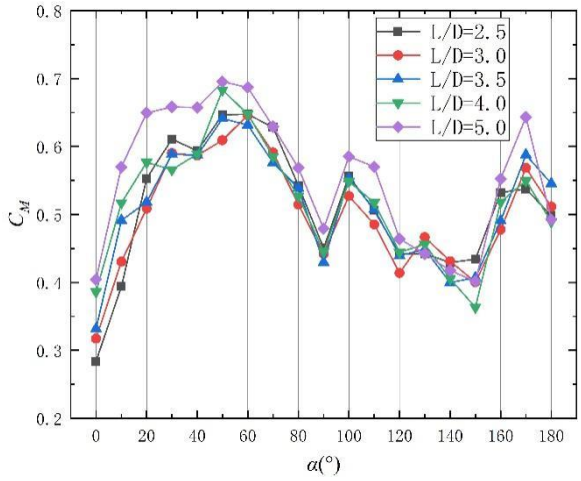

Fig. 27 Bending moment coefficient of downwind foundation of Building 2 at different spacing ratios and different wind directions

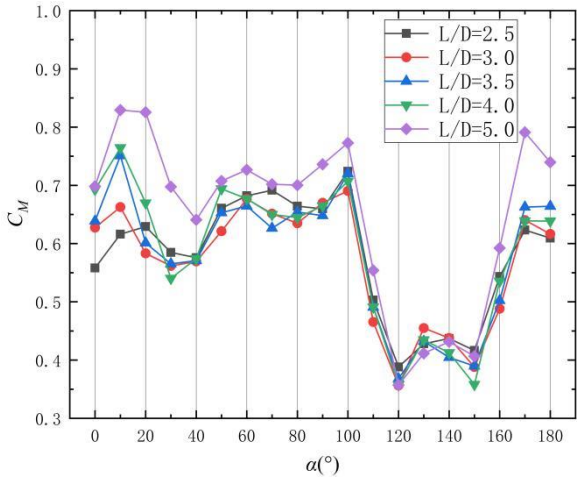

Fig. 29 Cross wind foundation moment coefficient of Building 2 under different spacing ratios and wind directions

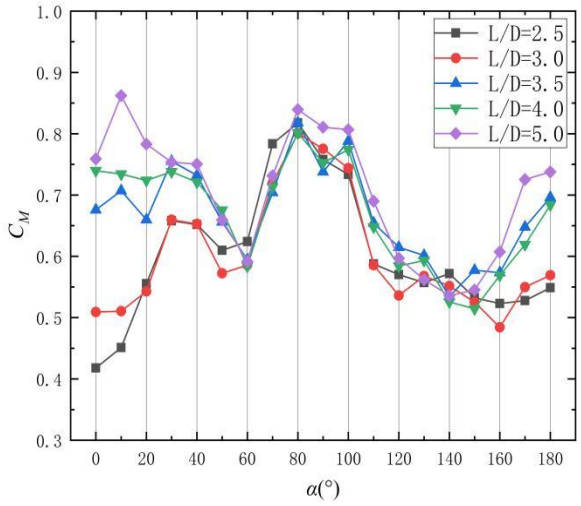

Fig. 28 Cross wind foundation moment coefficient of Building 1 under different spacing ratios and wind directions

wind direction angle range $30° \leq \alpha \leq 180°$, the variation trend of the transverse bending moment coefficient of the wind base under different spacing ratios is basically the same. In the interval of $0° \leq \alpha \leq 30°$, the difference value of the transverse wind base bending moment coefficient decreases with increasing angle at different wind direction ratios. Under the same wind direction, the transverse wind base bending moment coefficient increases with increasing distance ratio. The maximum transverse base bending moment coefficient of Building 1 is 0.862, the spacing ratio is 5.0, and the wind direction angle is 10°.

Figure 29 shows the bending moment coefficient of transverse wind base of Building 2 under different spacing ratios and wind angles. The bending moment coefficient of transverse wind base of Building 2 under different spacing ratios shows the same variation trend with the angles. In Building 2, the maximum bending moment coefficient of wind direction base is 0.829, the spacing ratio is 5.0, and the wind direction angle is 10°.

7. CONCLUSION

Through the rigid model pressure measurement wind tunnel test, the variation law of the size coefficient, fluctuating wind pressure coefficient and the bending moment coefficient of the base of the tall buildings with different spacing ratios and different wind direction in shape arrangement was tested and analyzed. The data of the working condition range measured in this test were analyzed and the main conclusions were obtained as follows:

i) For Building 1, the zoned shape coefficients of Planes I, F, G and J have the same variation rule of wind direction angle under different spacing ratios, and the zoned shape coefficients are less affected by the spacing ratio. Plane H is always under negative pressure. For different spacing ratios, the variation rule of wind direction angle of Plane H is different. For Building 2, the zoned shape coefficients of the three Planes K, L and M have the same wind direction angle change rule under different spacing ratios. Zoned shape coefficients are less affected by spacing ratios, while Planes N and P are more affected by spacing ratios.

ii) When the wind direction angle is 180º, the fluctuating wind pressure coefficient on both sides of Building 1 is most affected by the spacing ratio. At this wind direction angle, the maximum value is 0.43 when the spacing ratio is 5.0, which is 65% different from the minimum value. When the wind direction angle is 0º, the spacing ratio increased from 2.5 to 3.0, the maximum fluctuating wind pressure coefficient on the windward side of Building 2 can be reduced by about 29 %, thereafter, with increasing spacing ratio, the range of change is small.

iii) The maximum bending moment coefficient from Building 1 downwind to the base is 0.733, the spacing ratio is 5.0, and the wind direction angle is 40°. The maximum transverse base bending moment coefficient is 0.862, the spacing ratio is 5.0, and the wind direction angle is 10°. The maximum bending moment coefficient of Building 2 downwind to the base is 0.695, the spacing

ratio is 5.0, and the wind direction angle is 50°. The maximum transverse base bending moment coefficient is 0.829, the spacing ratio is 5.0, and the wind direction angle is 10°.

iv) For the pyramidal group of buildings, the interference effects on each face of the building under different spacing ratios and wind angles are favorable and unfavorable. Therefore, the optimal design scheme should be selected according to the most unfavorable state and interference state of the structure. The building spacing ratio should preferably be fixed at 3.0, and wind angles of 10°, 40° and 50° should be avoided as far as possible.

v) Systematic studies are desirable for high-rise buildings, which are significantly affected by wind and are expensive to build. In the future, it is advisable to build a wind load parameter database for common building section forms and building layout forms, to make them more targeted in practical applications. Ensuring a high level of construction safety, reducing its construction costs and saving resources.

ACKNOWLEDGEMENTS

The study is financially supported by Natural Science Foundation of Hebei Province (E2022210069), Natural Science Foundation of Hebei Province Innovative Research Group Project (E2022210078), National Natural Science Foundation of China (11802186,5177838), and Department of Education of Hebei Province (BJ2019004).

CONFLICT OF INTEREST

The authors declare no conflict of interest.

AUTHORS CONTRIBUTION

Conceptualization, H.C. and S.C.S.; Methodology, H.C., H.A. and M.M.; Validation, Z.H.; Formal analysis, H.A. and Z.H.; Resources, Z.H. and Q.L.; Data curation, M.M.; Writing—original draft, H.C.; Writing—review & editing, H.A., M.M., Z.H., Q.L. and S.C.S.; Visualization, H.C.; Supervision, Q.L. and S.C.S.; Project administration, Q.L. All authors have read and agreed to the published version of the manuscript.

REFERENCES

Bharat Singh, C., Chakrabarti, A. & A. K. Ahuja (2022). Study of wind loads on rectangular plan tall building under interference condition. *Structures*, 43, 105-130. https://doi.org/10.1016/j.istruc.2022.06.041

Chunyan, L., Zhang C. & Peng X. (2011). Numerical simulation of static interference effect of zigzag buildings. *Journal Huaqiao University (Natural Science,)* 32(1), 87-91.

Deqian, Z., Gu, M., Zhang, A., & J. Zhang (2011). Large eddy simulation of flow around a single square building model with 1:1:16 shape. *Journal of Vibration and Shock*, 35(5), 96-100. https://doi.org/10.13465/j.cnki.jvs.2011.05.046.

Dongmei, H., Zhu, L. & Chen, W. (2012). Amplitude characteristics of wind loads on high-rise buildings with interference from surrounding buildings. *China Civil Engineering Journal*, 45(9), 1-10.: https://doi.org/10.15951/j. tmgcxb.2012.09.016

GB50009 Load code for the design of building structures (2012) Architecture Industry Press Beijing, China.

Huaying, W., Li, T., Jiang, T. & H. Huang (2015). Numerical simulation and analysis on wind load shape coefficient of high-rise building. *Journal of East China Jiaotong University*, 32(2), 103-108. https://doi.org/10.16749/j.cnki.jecjtu.2015.02.014

Kunyang, L. (2021). Study on the interference effect of oblique tri-square column under average wind load. *Journal of Hunan City University (Natural Science)*, 30(6), 1-6. https://doi.org/10.3969/j.issn.1672-7304.2021.06.0001

Lam, K. M., Leung, M. Y. H., & Zhao, J. G. (2008). Interference effects on wind load of a row of closely spaced tall buildings. *Journal of Wind Engineering and Industrial Aerodynamics*, 96(5), 562-583. https://doi.org/10.1016/j.jweia.2008.01.010

Li, Z., & Y. Li (2022). The influent of multi/high-rise building on the surface wind load of low-rise building. *Alexandria Engineering Journal*, 61, 11979-11991. https://doi.org/10.1016/j.aej.2022.05.053

Liguo, Y., Yan, Y. & Zhou, Y. (2021). Wind tunnel study of wind-induced interference effects on high-rise buildings. *Building Science*, 37(11), 48-54. https://doi.org/10.13614/j.cnki.11 — 1962/tu.2019. 07. 011

Nagar, S. K., Raj, R. & Dev, N. (2022). Proximity effects between two plus-plan shaped high-rise buildings on mean and RMS pressure coefficients. *Scientia Iranica, A* 29(3), 990-1005. https://doi.org/10.24200/sci.2021.55928.4484

Qingkuan, L. (2011). Aerodynamic and structure desigh of m ultifunction boundary-layer wind tunnel. *Journal of Experiments in Fluid Mechanics*, 25(3), 66-70. https://doi.org/10.14006 /j.jzjgxb.2016.10.017

Rongqiang, D., Zhu, X., Li, Z. (2022). Study on interference effects of the cross-shaped super tall buildings in different distance. *Building Science*, 38(3), 103-110. https://doi.org/10.13614/j.cnki.11-1962/tu.2022.03.014

Rongyang, W., Lu, B., Zuo, X., Yan, L., Zhu, Y. & Wei, Y. (2022). Numerical computations of flow around three equilateral-triangular square cylinders with rounded corners using momentum exchange-based IB-LBM at low Reynolds numbers. *Ocean Engineering*, 263, 1-19. https://doi.org/10.1016/j.oceaneng.2022.112373

Weifeng, Q., Shi, J., Yang, X., Xie, J. & Zuo S. (2022). Characteristics of wind loads on Twin-Tower structure in comparison with single tower. *Engineering Structures*, 251, 1-21.

https://doi.org/10.1016/j.engstruct.2021.112780

Xiaobing, L., Yu, W., Wu, Q., Tao, T. & Yang Q. (2021). Experimental study on the aerodynamic characteristics of three side-by-side square cylinders. *Journal of Vibration and Shock*, 40(22), 75-97. https://doi.org/10.13465/j.cnki.jvs.2021.22.011

Yalin, Y., Tang, Y. & Yang, L. (2021). Wind-induced interference effect of array distributed high-rise buildings. *Building Science*, 37(11), 48-54. https://doi.org/10.13614/j.cnki.11-1962/tu.2021.11.007

Yi, T., Jin, X. & Yang, L. (2012). Study of the interference effects of wind loads on tall buildings in staggered arrangement. *China Civil Engineering Journal*, 45(8), 97-103. https://doi.org/10.15951/j.tmgcxb.2012.08.018

Zhuangning, X., Gu, M. & Ni, Z. (2003). Experimental study of wind load on three square prisms of side-by-side arrangements. *Journal of Xi'An JiaoTong University*, 37(3), 290-293.